Research Article | Vol. 29, No. 13 / 21 June 2021 / Optics Express 19506
Optics EXPRESS

Single-shot spatiotemporal characterization of a multi-PW laser using a multispectral wavefront sensing method

YEONG GYU KIM,[1,2] JI IN KIM,[1,2] JIN WOO YOON,[1,3] JAE HEE SUNG,[1,3] SEONG KU LEE,[1,3,4] AND CHANGE HEE NAM[1,2,5]

[1]Center for Relativistic Laser Science, Institute for Basic Science, Gwangju 61005, Republic of Korea
[2]Department of Physics and Photon Science, GIST, Gwangju 61005, Republic of Korea
[3]Ultraintense Laser Laboratory, Advanced Photonics Research Institute, GIST, Gwangju 61005, Republic of Korea
[4]lsk@gist.ac.kr
[5]chnam@gist.ac.kr

Abstract: The single-shot spatiotemporal characterization of an ultrahigh intensity laser pulse was performed using a multispectral wavefront sensor. For the measurement of the spatio-spectral electric field, a femtosecond laser pulse was spectrally modulated and separated by a Fabry-Perot etalon coupled with a grating pair, and its spatio-spectral electric field was measured with a wavefront sensor. The spatiotemporal electric field was reconstructed from the measured spatio-spectral electric field of a multi-PW laser pulse. We found that the spatiotemporal distortion could reduce the focused laser intensity by 15%, compared to the case of a diffraction-limited and transform-limited laser pulse.

© 2021 Optical Society of America under the terms of the OSA Open Access Publishing Agreement

1. Introduction

Ultrashort high-power lasers, based on the chirped pulse amplification (CPA) technique, have been developed [1,2] and applied for exploring laser-matter interactions under extreme physical conditions. In laser-matter interactions, laser intensity is one of the critical parameters to determine the interaction regime. With ultrahigh intensity lasers we can investigate laser-driven charged particle acceleration [3–5] and strong field quantum electrodynamics [6]. In order to obtain the highest achievable intensity from a high-power laser, a near diffraction-limited focusing is desired with a laser pulse width close to the transform-limited duration [7,8]. Since the quality of a laser relies on its temporal and spatial properties, the position-dependent temporal variation, called as spatiotemporal coupling (STC) [9], should be characterized to determine the quality of a laser and to achieve its best performance.

Due to the importance of STC, such as pulse front tilt and radial group delay, intensive investigations on STC have been performed in various fields [10,11]. In CPA lasers, the study on STC began with particular problems originating from such optical elements as a grating [12–14] and a beam expander [15–17]. A misaligned grating, in a pulse stretcher or a compressor, can induce a pulse front tilt to the laser pulse. In addition, a surface distortion in a grating pulse compressor can produce complex spatiotemporal distortion [18–21]. If the chromatic aberration of a beam expander, installed to increase the beam size, is not properly eliminated, a radial group delay can be generated. The STC can increase the spot size and also the pulse duration at the focus, which significantly reduces the achievable laser intensity [19–24]. Consequently, the precise measurement and the control of STC are critical for achieving the best performance of an ultrahigh-power laser [25,26].

A complete spatiotemporal electric field, $E(x, y, t)$, of an ultrahigh-power laser is difficult to measure due to the limitation in detection dimension (≤2-D). This limitation restricts the

#429891 https://doi.org/10.1364/OE.429891
Journal © 2021 Received 27 Apr 2021; revised 30 May 2021; accepted 31 May 2021; published 8 Jun 2021

Optics EXPRESS

extension of temporal measurement techniques to the 2-D spatiotemporal measurement, $E(x, t)$ [27] or $E(r, t)$ [28], including only one spatial axis. For the complete spatiotemporal detection, $E(x, y, t)$, of a laser pulse using a 2-D device, special techniques have been developed [29–36]. In order to expand the dimension of measurement to 3-D, a spatial scan [29,30] or delay scan [31] is adopted. By scanning the delay line, the cross correlation function, $S(x, y, \omega)$, is obtained, which can be converted to spectrally resolved 3-D data, $E(x, y, \omega)$ [31]. Since this technique requires more than thousand laser shots, iteration techniques were developed to reduce the number of required shots [32,33].

Unlike the scanning method, a frequency-resolved wavefront sensing method [34] can reduce the required shot number by employing a snap-shot multispectral imaging technique that links the spatial registration with wavelength [35,36]. The first demonstration of single-shot measurement used a coarse diffractive optical element and a variable bandpass filter [35]. Another single-shot wavefront sensing technique uses a mosaic bandpass filter, where three bandpass filters with different colors were periodically placed in front of a wavefront sensor, such as a RGB camera [36]. By selecting the same color pixels, the spatio-spectral components could be reconstructed. Such a single-shot technique is essential for diagnosing high-power lasers operating at low-repetition rate.

In this paper, we present a simple, complete 3-D spatiotemporal measurement technique that utilizes a Fabry-Perot etalon, two gratings, and a wavefront sensor. Using the developed sensor, we demonstrated the characterization of an ultrahigh-power laser pulse generated by tightly focusing a multi-PW laser with an $f/1.1$ off-axis parabolic mirror. From the measured 3-D electric field, we calculated the STC, estimated the peak intensity at focus, and compared with that of a diffraction-limited and transform-limited pulse, evaluating the quality of an ultrahigh-power laser in a single-shot.

2. Single-shot multispectral wavefront sensing technique

The spatiotemporal electric field of a laser pulse can be obtained through the Fourier transform of a spatio-spectral electric field. In this measurement technique, a set of spatio-spectral data at several frequencies is measured and the continuous spatio-spectral intensity, $I(x, y, \omega)$, and phase, $\phi(x, y, \omega)$, can be obtained from the interpolation and extrapolation. Then, a continuous spatio-spectral electric field is obtained as,

$$E(x, y, \omega) = \sqrt{I(x, y, \omega)} \exp[i\phi(x, y, \omega) + i\varphi(\omega)], \tag{1}$$

where $\varphi(\omega)$ is the spectral phase. After the construction of a continuous 3-D spatio-spectral data, a Fourier transform is applied along the frequency axis to obtain the 3-D spatiotemporal electric field of a laser pulse,

$$E(x, y, t) = \frac{1}{2\pi} \int_{-\infty}^{\infty} E(x, y, \omega) \exp[-i\omega t]\, d\omega. \tag{2}$$

From the spatio-spectral electric field, the spatiotemporal electric field of a high-power femtosecond laser pulse can be obtained in Eq. (2).

For the single-shot characterization of the spatiotemporal electric field, $E(x, y, t)$, of a multi-PW laser pulse, the spatio-spectral electric field, $E(x, y, \omega)$, was measured at a set of selected wavelengths. In order to obtain the spatio-spectral electric field, a spectrum of the laser pulse was selected by an etalon, and then the laser pulse was spectrally dispersed using a pair of transmission gratings. Consequently, with the combination of the etalon and the pair of gratings, as shown in Fig. 1, the spatio-spectral electric field can be obtained at a set of transmitted wavelengths in a single-shot.

Optics EXPRESS

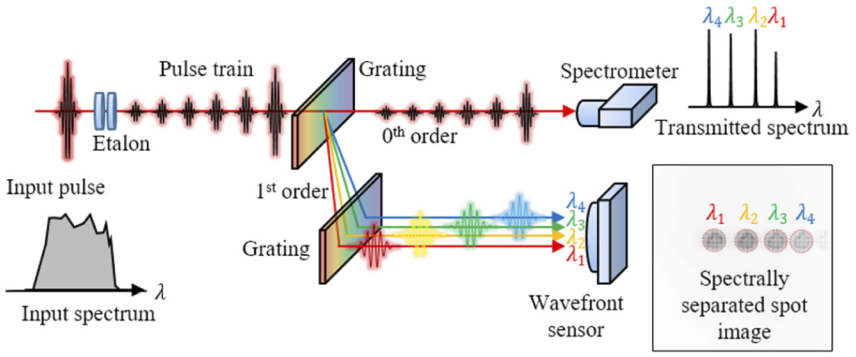

Fig. 1. Schematics of the multispectral wavefront sensor and spectrally separated spot image. δ_1, δ_2, δ_3, and δ_4: transmitted wavelengths from the etalon.

3. Experimental setup

With the multispectral wavefront sensing device, the spatiotemporal electric field of the multi-PW laser at Center for Relativistic Laser Science was measured and the spatiotemporal electric field generated by focusing a multi-PW laser pulse with an off-axis parabolic mirror was estimated. For reconstructing of a full 3-D electric field, the central part of a laser beam is picked off and the spectral phase, shown in Fig. 2(a), was measured by spectral phase interferometry for direct electric-field reconstruction device (APE, FC-SPIDER). The schematic diagram of the beam path from the deformable mirror, installed after the pulse compressor, to the measurement device is shown in Fig. 2(b). The laser beam on the deformable mirror DM (AKA optics, 320 mm, 127 electrodes) was relay-imaged to the position of the achromatic telescope T with M=1/3 with the f/1.1 off-axis parabolic mirror OAP (Aperture Optical Science, focal length: 300 mm), the apochromatic objective lens L1 (magnification: 50, focal length: 4 mm), and two achromatic doublets (L2 and L3 with focal length 300 and 500 mm, respectively). Because of the 1/3x Galilean telescope placed at the position T, the virtual image was relayed by the two achromatic doublets (L4 and L5 with focal length 1000 and 750 mm, respectively), arranged as a Kepler telescope of magnification of 0.75. As a result, the intensity and phase at the position DM1 could be relay-imaged onto the wavefront sensor with the magnification of 1/180. After the final relaying lens, a piezo-type etalon (Light Machinery, free spectral range 10 THz) is placed to modulate the laser spectrum to a set of discrete spectral components. The transmitted spectra can be easily tuned by changing the piezo-voltage applied to the etalon. The spectrally modulated laser beam was then separated by the transmission grating pair (Thorlabs, GTI25-03A). The input angle of the grating pair was set to the Littrow angle at the center wavelength (7.0° at 808 nm) because the aberration induced by the grating pair is reduced when the diffraction angle was close to the input angle [37]. The Littrow angle is not a constant for a broadband laser, and hence chromatic aberration occurs at the sideband. To reduce the chromatic aberration, low groove density (300 grooves/mm) is selected. The transmitted 0th-order beam of the first grating was monitored with a spectrometer to obtain the transmitted spectrum of the etalon. The modulated and separated laser beam was measured by the Shack-Hartmann type wavefront sensor (AKA Optics), as shown in Fig. 1. The number of microlenses was 147×147 with an array pitch of the wavefront sensor of 103.6 μm, the aperture dimension of 15.2×15.2 mm^2, and the measurement accuracy of 3.5 nm. During the measurement, an active feedback loop between the deformable mirror and the wavefront sensor was disabled.

Optics EXPRESS

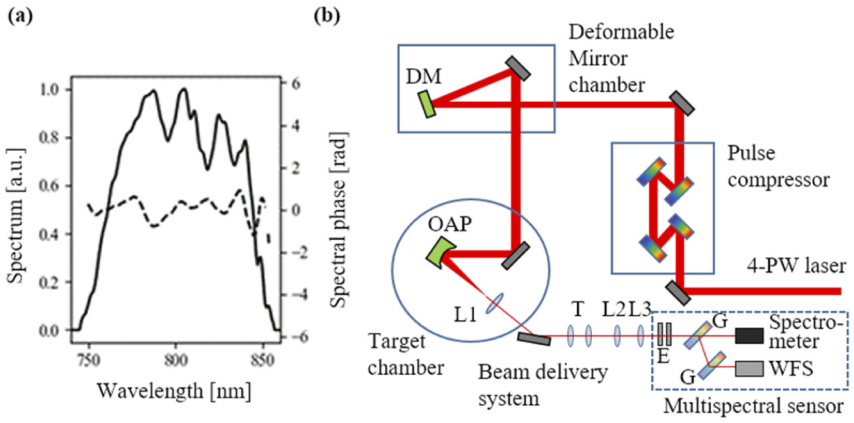

Fig. 2. (a) Spectrum and spectral phase of a multi-PW laser pulse. (b) Schematics of the measurement setup for characterizing the spatiotemporal electric field of a multi-PW laser pulse. DM: deformable mirror, OAP: off-axis parabolic mirror, T: telescope, L: lens, G: grating, E: etalon, and WFS: wavefront sensor.

4. Results and discussion

4.1. Spatiotemporal characteristics of the multi-PW laser

For the measurement of the spatiotemporal properties of multi-PW laser pulses, the spatio-spectral data was obtained using the developed multispectral wavefront sensor. Four spatio-spectral components of a multi-PW laser pulse were spectrally separated by the grating pair and the etalon. From the spectrally separated spot image of the four spatio-spectral components at 830, 808, 788, and 771 nm recorded on the wavefront sensor, as shown in the Fig. 3(a), the spatio-spectral intensity and phase at each wavelength were obtained. The intensity was obtained by applying a low-pass filter to the spot image, and the phase was obtained from the displacement of the spot positions with respect to the reference positions [38]. The obtained and spatio-spectral intensity and phase profiles, shown in Fig. 3(b) and (c), at different wavelengths show fairly similar shapes. This indicates that strong spatiotemporal coupling did not occur in the multi-PW laser pulse.

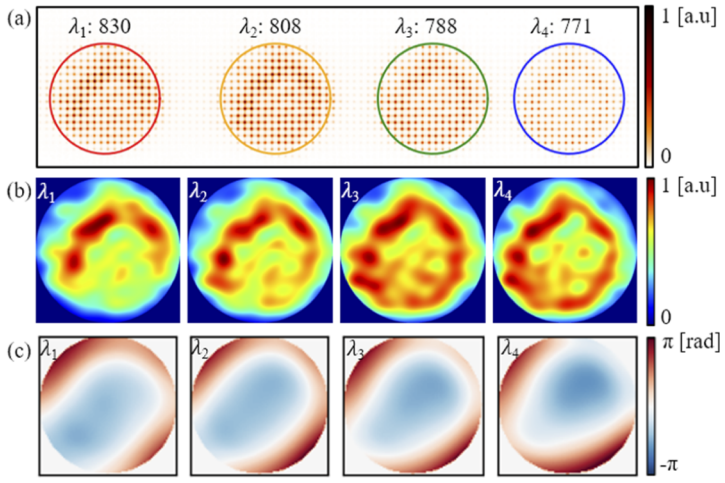

Fig. 3. (a) Spectrally separated spot image. Wavelength-resolved spatio-spectral intensity profiles (b) and phases (c) at the wavelengths of 830, 808, 788, and 771 nm.

Optics EXPRESS

For the detailed analysis, the spatiotemporal electric field, $E(x, y, t)$, of a multi-PW laser pulse was reconstructed by applying Eq. (2) to the spatio-spectral data, $E(x, y, \omega)$. The 20% and 50% isosurfaces of the peak intensity of the reconstructed spatiotemporal intensity, $I(x, y, t)$, is shown for each case in Fig. 4(a-i). Figure 4(a-ii), (a-iii), and (a-iv) shows isosurfaces with the different spectral component set to examine the validity of the measurement. This is discussed in detail in Sec. 4.2. From the reconstructed data, the retrieved position-dependent temporal characteristics of the laser pulse showed that the pulse width variation in space is small. The average value and the standard deviation of the pulse width in the pupil area of the laser beam were 22.1 fs and 0.4 fs, respectively. The pulse front tilt was estimated to be dt_0/dx = 0.032 fs/mm and dt_0/dy = 0.067 fs/mm. This pulse front tilt can be compensated for by eliminating the angular dispersion through the fine-tuning of the pulse compressor [27,39]. The detailed procedure of eliminating this kind of pulse front tilt in our multi-PW laser was presented in our earlier work [7]. The estimation of radial group delay was found to be negligible, because an achromatic lens and reflective type mirrors were employed in the beam expanders of the multi-PW laser. The reconstruction of the near-field spatiotemporal electric field, thus, showed that the performance of the multi-PW laser was not affected significantly by the spatiotemporal coupling.

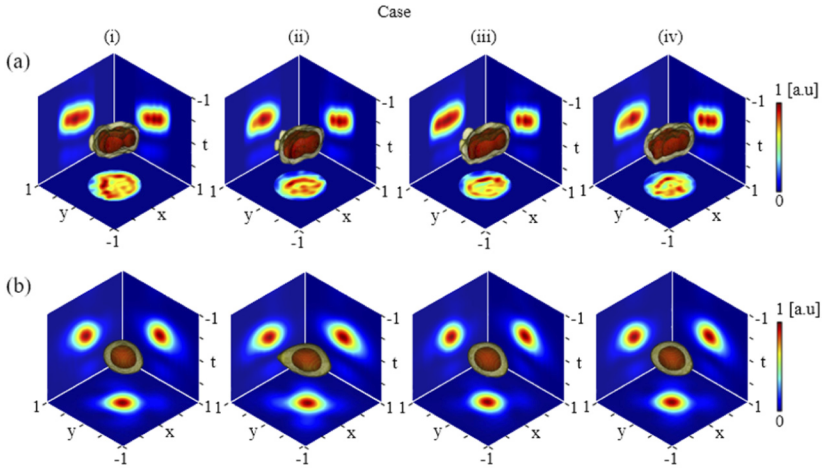

Fig. 4. 3-D representation of the spatiotemporal intensity of PW laser pulses at (a) the near-field and (b) the focus, with the images projected along the x-, y-, and t-axes. (i)-(iv) show the spatiotemporal intensity for the four different spectral component sets: (i) 771, 788, 808, and 830 nm, (ii) 768, 787, 808, and 832 nm, (iii) 767, 786, 808, and 833 nm, and (iv) 775, 795, 817, and 843 nm. The x- and y-axes in (a) and (b) are normalized to the pupil diameter and the diffraction-limited spot diameter, respectively. The t-axis is normalized to the duration of 50 fs. The spatiotemporal intensity is plotted as isosurfaces set at 20% and 50% of the peak intensity, respectively.

From the spatiotemporal electric field, $E(x, y, t)$, of a multi-PW laser pulse at the near-field, the spatiotemporal electric field at the focal plane can be reconstructed using the unidirectional pulse propagation equation [40]. In the reconstruction, the average defocus was omitted since the average defocus can be easily eliminated by controlling the deformable mirror. The reconstructed spatiotemporal intensity in Fig. 4(b-i) shows that the laser pulse is well bunched in the space and time domain. The most critical parameter of a laser pulse is the peak intensity achievable at the focus. For the estimation of the effect of the spatiotemporal coupling to the pulse duration and the peak intensity at the focus, the four focal spot parameters, the full effective pulse duration $T_{\mathrm{eff,full}}$ [41], the spatiotemporal effective pulse duration $T_{\mathrm{eff,STC}}$, and full spatiotemporal Strehl

Optics EXPRESS

ratio SR_{full}, and spatiotemporal Strehl ratio SR_{STC} [42], are defined as follows:

$$T_{\text{eff,full}} = \int_{-\infty}^{\infty} \frac{\int_{-\infty}^{\infty}\int_{-\infty}^{\infty} I(x,y,t)dxdy}{\max\left[\int_{-\infty}^{\infty}\int_{-\infty}^{\infty} I(x,y,t)dxdy\right]}dt, \tag{3}$$

$$T_{\text{eff,STC}} = \int_{-\infty}^{\infty} \frac{\int_{-\infty}^{\infty}\int_{-\infty}^{\infty} I_{\text{STC}}(x,y,t)dxdy}{\max\left[\int_{-\infty}^{\infty}\int_{-\infty}^{\infty} I(x,y,t)dxdy\right]}dt, \tag{4}$$

$$SR_{\text{full}} = \frac{\max[I(x,y,t)]}{\max[I_{\text{DL,TL}}(x,y,t)]}, \tag{5}$$

and

$$SR_{\text{STC}} = \frac{\max[I_{\text{STC}}(x,y,t)]}{\max[I_{\text{DL,TL}}(x,y,t)]}, \tag{6}$$

where $I_{\text{DL,TL}}$ denotes the intensity of a diffraction-limited and transform-limited pulse, and I_{STC} is the intensity of the laser pulse with zero frequency-averaged spatio-spectral phase, $\phi(x,y,\omega)$, and spectral phase, $\varphi(\omega)$. After compensating for the average spatio-spectral phase and the spectral phase with a deformable mirror and an acousto-optic programmable dispersive filter, the residual spatiotemporal coupling leads to the degradation of the focal spot parameters. For comparison, the case of a diffraction-limited and transform–limited ideal pulse is also calculated. From the reconstructed spatiotemporal electric field at the focus, we obtained $T_{\text{eff,full}}$ and $T_{\text{eff,STC}}$ to be 32.3 fs and 26.6 fs, respectively, which are 38% and 14% larger compared to the effective pulse duration, 23.4 fs, of the ideal pulse. The SR_{full} of the multi-PW laser pulse is 0.52, i.e. the peak intensity of the laser pulse at the focus is lower by 48% than that of the ideal pulse. The spatiotemporal Strehl ratio, SR_{STC}, representing the effect of the spatiotemporal coupling to the intensity at the focus was 0.85, indicating that the spatiotemporal coupling reduced the peak intensity by 15%, as compared to the ideal case.

4.2. Validity analysis

In the validity analysis, two types of potential errors were considered. As the measurement with a finite number of spectral components can lead to erroneous interpretation, the measurement with four spectral components should be validated. This kind of measurement is strongly influenced by the quality of a laser pulse. For example, if the spectral component of a laser pulse includes only linear variation, such as linear angular dispersion and linear radial group delay, three components are enough to inspect their existence [36]. On the other hand, a complex spatiotemporal coupling can induce complex spatio-spectral aberrations [18–21], which requires more than three spectral components with smaller sampling interval.

First, consider the case that the spectral phase is smooth, but varies rapidly, shown in Fig. 5(a). This type of error is bounded by the second-order derivatives and the measurement spacing [30]:

$$|\psi(x,y,\omega) - \phi(x,y,\omega)| \le \frac{(\omega_i - \omega_{i+1})^2}{8} \max|\psi''(x,y,\omega)|, \tag{7}$$

where $\omega_i<\omega<\omega_{i+1}$, Ψ is the actual spatio-spectral phase, and ϕ is the interpolated spatio-spectral phase. As the actual spatio-spectral phase of the laser pulse was not known, its second derivative was approximated with the Lagrangian polynomial constructed from the measured data [43]:

$$\psi''(x,y,\omega) \approx L''(x,y,\omega). \tag{8}$$

The RMS value of the estimated error bound over the pupil area was 72 mrad (1/87 wave), so the effect of the error was almost negligible in the reconstruction of the spatiotemporal electric field of a laser pulse.

Optics EXPRESS

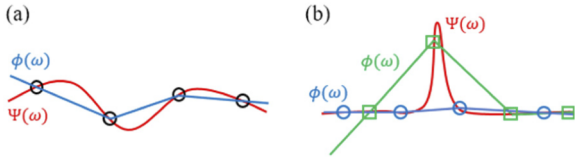

Fig. 5. (a) The first case with a rapidly varying spectral phase, shown in the red line. The black circles show the measurement of a spectral phase at four wavelengths. The blue line shows the linear interpolation of the measured data. (b) The second case with a sharply peaked spectral phase, shown in the red line. The blue and the green curves are the linear interpolations of two different measurements shown as the blue circles and the green rectangles.

The second type of error, shown in Fig. 5(b), cannot be dealt with Eqs. (7) and (8). In order to examine this type of error, the data from the four sets of measurements with tuned transmitted spectra, listed in Table 1, were analyzed. The wavelength selection of the transmitted spectra was made by adjusting the mirror spacing of the etalon. If there exists the second type of error, the difference in the reconstructed result may appear when reconstructing with different spectral components. The 20% and 50% isosurfaces of the peak intensity of the reconstructed spatiotemporal intensity for the four cases are shown in Fig. 4. In the near field, the average pulse width over the pupil area ranged from 22.0 to 22.1 fs and its standard deviations varied from 0.4 to 0.6 fs. At the focus, the SR_{STC} of the four cases ranged from 0.85 to 0.90 with the average value of 0.88. The reconstructed spatiotemporal electric field, thus, showed no significant difference. Consequently, the reconstruction result did not show any sign of the second type error.

Table 1. Wavelength table of four measurements

	δ_1 [nm]	δ_2 [nm]	δ_3 [nm]	δ_4 [nm]
(i)	830	808	788	771
(ii)	832	808	787	768
(iii)	833	808	786	767
(iv)	843	817	795	775

5. Conclusion

We developed a single-shot 3-D spatiotemporal measurement device to obtain the spatiotemporal electric field of an ultrahigh intensity laser pulse produced by tightly focusing a multi-PW laser with an $f/1.1$ optics. For the measurement of the spatiotemporal electric field, a femtosecond laser pulse was spectrally separated by an etalon coupled with a grating pair, and its spatio-spectral electric field was measured with a wavefront sensor. From the reconstructed spatiotemporal electric field, the spatiotemporal Strehl ratio, SR_{STC}, was 0.85, indicating that the intensity degradation of the multi-PW laser pulse due to the spatiotemporal coupling was not severe. The error analysis performed to ensure the validity of our measurement showed that the estimated measurement error was negligible. Consequently, the developed spatiotemporal measurement device can be widely applied to the spatiotemporal characterization of ultrahigh intensity lasers.

Funding. Institute for Basic Science (IBS-R012-D1); Gwangju Institute of Science and Technology (Ultrashort Quantum Beam Facility (UQBF) operation program (140011) through Advanced Photonics Research Institute).

Disclosures. The authors declare no conflicts of interest.

Data availability. Data underlying the results presented in this paper are not publicly available at this time but may be obtained from the authors upon reasonable request.

Optics EXPRESS

References

1. J. H. Sung, H. W. Lee, J. Y. Yoo, J. W. Yoon, C. W. Lee, J. M. Yang, Y. J. Son, Y. H. Jang, S. K. Lee, and C. H. Nam, "4.2 PW, 20 fs Ti:sapphire laser at 0.1 Hz," Opt. Lett. **42**(11), 2058–2061 (2017).
2. C. N. Danson, C. Haefner, J. Bromage, T. Butcher, J.-C. F. Chanteloup, E. A. Chowdhury, A. Galvanauskas, L. A. Gizzi, J. Hein, D. I. Hillier, N. W. Hopps, Y. Kato, E. A. Khazanov, R. Kodama, G. Korn, R. Li, Y. Li, J. Limpert, J. Ma, C. H. Nam, D. Neely, D. Papadopoulos, R. R. Penman, L. Qian, J. J. Rocca, A. A. Shaykin, C. W. Siders, C. Spindloe, S. Szatmári, R. M. G. M. Trines, J. Zhu, P. Zhu, and J. D. Zuegel, "Petawatt and exawatt class lasers worldwide," High Power Laser Sci. Eng. **7**, e54 (2019).
3. H. T. Kim, K. H. Pae, H. J. Cha, I. J. Kim, T. J. Yu, J. H. Sung, S. K. Lee, T. M. Jeong, and J. Lee, "Enhancement of Electron Energy to the Multi-GeV Regime by a Dual-Stage Laser-Wakefield Accelerator Pumped by Petawatt Laser Pulses," Phys. Rev. Lett. **111**(16), 165002 (2013).
4. I. J. Kim, K. H. Pae, C. M. Kim, H. T. Kim, J. H. Sung, S. K. Lee, T. J. Yu, I. W. Choi, C.-L. Lee, K. H. Nam, P. V. Nickles, T. M. Jeong, and J. Lee, "Transition of Proton Energy Scaling Using an Ultrathin Target Irradiated by Linearly Polarized Femtosecond Laser Pulses," Phys. Rev. Lett. **111**(16), 165003 (2013).
5. W. J. Ma, I. J. Kim, J. Q. Yu, I. W. Choi, P. K. Singh, H. W. Lee, J. H. Sung, S. K. Lee, C. Lin, Q. Liao, J. G. Zhu, H. Y. Lu, B. Liu, H. Y. Wang, R. F. Xu, X. T. He, J. E. Chen, M. Zepf, J. Schreiber, X. Q. Yan, and C. H. Nam, "Laser Acceleration of Highly Energetic Carbon Ions Using a Double-Layer Target Composed of Slightly Underdense Plasma and Ultrathin Foil," Phys. Rev. Lett. **122**(1), 014803 (2019).
6. A. Di Piazza, C. Müller, K. Z. Hatsagortsyan, and C. H. Keitel, "Extremely high-intensity laser interactions with fundamental quantum systems," Rev. Mod. Phys. **84**(3), 1177–1228 (2012).
7. J. W. Yoon, C. Jeon, J. Shin, S. K. Lee, H. W. Lee, I. W. Choi, H. T. Kim, J. H. Sung, and C. H. Nam, "Achieving the laser intensity of 5.5×10^{22} W/cm^2 with a wavefront-corrected multi-PW laser," Opt. Express **27**(15), 20412–20420 (2019).
8. S. W. Bahk, P. Rousseau, T. A. Planchon, V. Chvykov, G. Kalintchenko, A. Maksimchuk, G. A. Mourou, and V. Yanovsky, "Generation and characterization of the highest laser intensities (10^{22} W/cm^2)," Opt. Lett. **29**(24), 2837–2839 (2004).
9. S. Akturk, X. Gu, P. Gabolde, and R. Trebino, "The general theory of first-order spatio-temporal distortions of Gaussian pulses and beams," Opt. Express **13**(21), 8642–8661 (2005).
10. C. Dorrer, "Spatiotemporal Metrology of Broadband Optical Pulses," IEEE J. Sel. Top. Quantum Electron. **25**(4), 1–16 (2019).
11. S. W. Jolly, O. Gobert, and F. Quéré, "Spatio-temporal characterization of ultrashort laser beams: a tutorial," J. Opt. **22**(10), 103501 (2020).
12. C. Fiorini, C. Sauteret, C. Rouyer, N. Blanchot, S. Seznec, and A. Migus, "Temporal aberrations due to misalignments of a stretcher-compressor system and compensation," IEEE J. Quantum Electron. **30**(7), 1662–1670 (1994).
13. G. Pretzler, A. Kasper, and K. J. Witte, "Angular chirp and tilted light pulses in CPA lasers," Appl. Phys. B **70**(1), 1–9 (2000).
14. Z. Bor, B. Racz, G. Szabo, M. Hilbert, and H. A. Hazim, "Femtosecond pulse front tilt caused by angular dispersion," Opt. Eng. **32**(10), 2501–2504 (1993).
15. Z. Bor, "Distortion of femtosecond laser pulses in lenses," Opt. Lett. **14**(2), 119–121 (1989).
16. S.-W. Bahk, J. Bromage, and J. D. Zuegel, "Offner radial group delay compensator for ultra-broadband laser beam transport," Opt. Lett. **39**(4), 1081–1084 (2014).
17. Z. Li and J. Kawanaka, "Efficient method for determining pulse-front distortion in an ultra-intense laser," J. Opt. Soc. Am. B **37**(9), 2595–2603 (2020).
18. J. Qiao, J. Papa, and X. Liu, "Spatio-temporal modeling and optimization of a deformable-grating compressor for short high-energy laser pulses," Opt. Express **23**(20), 25923–25934 (2015).
19. Z. Li, K. Tsubakimoto, H. Yoshida, Y. Nakata, and N. Miyanaga, "Degradation of femtosecond petawatt laser beams: Spatio-temporal/spectral coupling induced by wavefront errors of compression gratings," Appl. Phys. Express **10**(10), 102702 (2017).
20. A. Jeandet, A. Borot, K. Nakamura, S. W. Jolly, A. J. Gonsalves, C. Tóth, H.-S. Mao, W. P. Leemans, and F. Quéré, "Spatio-temporal structure of a petawatt femtosecond laser beam," JPhys Photonics **1**(3), 035001 (2019).
21. V. Leroux, T. Eichner, and A. R. Maier, "Description of spatio-temporal couplings from heat-induced compressor grating deformation," Opt. Express **28**(6), 8257–8265 (2020).
22. Z. Li and J. Kawanaka, "Complex spatiotemporal coupling distortion pre-compensation with double-compressors for an ultra-intense femtosecond laser," Opt. Express **27**(18), 25172–25186 (2019).
23. Z. Li, N. Miyanaga, and J. Kawanaka, "Theoretical comparison of spatiotemporal contrasts of pulsed beams in unfocusing, 1D-focusing, and 2D-focusing fields and enhancement of the on-axis temporal contrast at the focus," J. Opt. Soc. Am. B **35**(8), 1861–1870 (2018).
24. C. Bourassin-Bouchet, M. Stephens, S. de Rossi, F. Delmotte, and P. Chavel, "Duration of ultrashort pulses in the presence of spatio-temporal coupling," Opt. Express **19**(18), 17357–17371 (2011).
25. P. Zhu, X. Xie, J. Kang, Q. Yang, H. Zhu, A. Guo, M. Sun, Q. Gao, Z. Cui, X. Liang, S. Yang, D. Zhang, and J. Zhu, "Systematic study of spatiotemporal influences on temporal contrast in the focal region in large-aperture broadband ultrashort petawatt lasers," High Power Laser Sci. Eng. **6**, e8 (2018).

Optics EXPRESS

26. D. N. Papadopoulos, J. P. Zou, C. Le Blanc, G. Chériaux, P. Georges, F. Druon, G. Mennerat, P. Ramirez, L. Martin, A. Fréneaux, A. Beluze, N. Lebas, P. Monot, F. Mathieu, and P. Audebert, "The Apollon 10 PW laser: experimental and theoretical investigation of the temporal characteristics," High Power Laser Sci. Eng. **4**, e34 (2016).
27. K. Osvay, A. P. Kovacs, Z. Heiner, G. Kurdi, J. Klebniczki, and M. Csatari, "Angular dispersion and temporal change of femtosecond pulses from misaligned pulse compressors," IEEE J. Sel. Top. Quantum Electron. **10**(1), 213–220 (2004).
28. F. Wu, Y. Xu, Z. Li, W. Li, J. Lu, C. Wang, Y. Li, Y. Liu, X. Lu, Y. Peng, D. Wang, Y. Leng, and R. Li, "A novel measurement scheme for the radial group delay of large-aperture ultra-short laser pulses," Opt. Commun. **367**, 259–263 (2016).
29. P. Bowlan, P. Gabolde, and R. Trebino, "Directly measuring the spatio-temporal electric field of focusing ultrashort pulses," Opt. Express **15**(16), 10219–10230 (2007).
30. B. Alonso, ÍJ Sola, Ó Varela, J. Hernández-Toro, C. Méndez, J. San Román, A. Zaïr, and L. Roso, "Spatiotemporal amplitude-and-phase reconstruction by Fourier-transform of interference spectra of high-complex-beams," J. Opt. Soc. Am. B **27**(5), 933–940 (2010).
31. M. Miranda, M. Kotur, P. Rudawski, C. Guo, A. Harth, A. L'Huillier, and C. L. Arnold, "Spatiotemporal characterization of ultrashort laser pulses using spatially resolved Fourier transform spectrometry," Opt. Lett. **39**(17), 5142–5145 (2014).
32. G. Pariente, V. Gallet, A. Borot, O. Gobert, and F. Quéré, "Space–time characterization of ultra-intense femtosecond laser beams," Nat. Photonics **10**(8), 547–553 (2016).
33. A. Borot and F. Quéré, "Spatio-spectral metrology at focus of ultrashort lasers: a phase-retrieval approach," Opt. Express **26**(20), 26444–26461 (2018).
34. C. P. Hauri, J. Biegert, U. Keller, B. Schaefer, K. Mann, and G. Marowski, "Validity of wave-front reconstruction and propagation of ultrabroadband pulses measured with a Hartmann–Shack sensor," Opt. Lett. **30**(12), 1563–1565 (2005).
35. P. Gabolde and R. Trebino, "Single-shot measurement of the full spatio-temporal field of ultrashort pulses with multi-spectral digital holography," Opt. Express **14**(23), 11460–11467 (2006).
36. C. Dorrer and S. W. Bahk, "Spatio-spectral characterization of broadband fields using multispectral imaging," Opt. Express **26**(25), 33387–33399 (2018).
37. N. Delen and B. Hooker, "Verification and comparison of a fast Fourier transform-based full diffraction method for tilted and offset planes," Appl. Opt. **40**(21), 3525–3531 (2001).
38. L. Seifert, J. Liesener, and H. J. Tiziani, "The adaptive Shack–Hartmann sensor," Opt. Commun. **216**(4-6), 313–319 (2003).
39. A. Börzsönyi, L. Mangin-Thro, G. Cheriaux, and K. Osvay, "Two-dimensional single-shot measurement of angular dispersion for compressor alignment," Opt. Lett. **38**(4), 410–412 (2013).
40. M. Kolesik, J. V. Moloney, and M. Mlejnek, "Unidirectional Optical Pulse Propagation Equation," Phys. Rev. Lett. **89**(28), 283902 (2002).
41. A. S. Pirozhkov, Y. Fukuda, M. Nishiuchi, H. Kiriyama, A. Sagisaka, K. Ogura, M. Mori, M. Kishimoto, H. Sakaki, N. P. Dover, K. Kondo, N. Nakanii, K. Huang, M. Kanasaki, K. Kondo, and M. Kando, "Approaching the diffraction-limited, bandwidth-limited Petawatt," Opt. Express **25**(17), 20486–20501 (2017).
42. J. Bromage, C. Dorrer, and J. D. Zuegel, "Angular-dispersion-induced spatiotemporal aberrations in noncollinear optical parametric amplifiers," Opt. Lett. **35**(13), 2251–2253 (2010).
43. J. D. Hoffman and S. Frankel, *Numerical methods for engineers and scientists* (CRC press, 2018).

203.230.52.4 on 2024-09-10 09:04 UTC